photonics

MDPI

Article

Bend Distortion and Thermal Lensing Effect on Transverse Mode Instability

Dan Cheng [1,†], Qing Zhong [2,†], Yujun Feng [3,*], Kun Zhang [1,*], Zhaochen Cheng [1], Dayong Zhang [1] and Hong Zhao [1]

[1] No.11th Research Institute of China Electronics Technology Group Corporation, Science and Technology on Solid-State Laser Laboratory, Beijing 100061, China; dcheng@bjtu.edu.cn (D.C.); chengzhaochenemail@163.com (Z.C.); zdyzdy75@163.com (D.Z.)
[2] Graduate School of China Academy of Engineering Physics, Beijing 100088, China; qingks@aliyun.com
[3] Institute of Applied Electronics, China Academy of Engineering Physics (CAEP), Mianyang 621900, China
* Correspondence: fabius769@163.com (Y.F.); nukzhang@163.com (K.Z.)
† These authors contributed equally to this work.

Abstract: In this work, we conducted a numerical analysis to investigate the combined effect of thermal lensing and bending-induced mode distortion on transverse mode instability in conventional large-mode-area (LMA) step-index fibers. Utilizing the finite element method, conformal mapping, and thermal conduction equations, we simulated the mode profiles in LMA 20/400 and 25/400 fibers subjected to both bending and thermal lensing effects; the corresponding evolution of mode loss and effective area were explored as well. Additionally, by introducing the derived mode profiles to the TMI coefficient calculations, we analyzed the influence of bending and thermal lensing (TL) on TMI; the simulation results indicate that the mode distortion caused by bending and the TL effect, under the bending conditions commonly encountered in practice, do not have pronounced impacts on TMI coefficient and TMI threshold.

Keywords: transverse mode instability; thermal lensing; mode distortion

Citation: Cheng, D.; Zhong, Q.; Feng, Y.; Zhang, K.; Cheng, Z.; Zhang, D.; Zhao, H. Bend Distortion and Thermal Lensing Effect on Transverse Mode Instability. *Photonics* **2024**, *11*, 1104. https://doi.org/10.3390/photonics11121104

Received: 7 October 2024
Revised: 18 November 2024
Accepted: 19 November 2024
Published: 22 November 2024

1. Introduction

Fiber laser systems have demonstrated significant advancements in power scalability. The exceptional surface-to-volume ratios of fiber geometries contribute to their remarkable thermal handling capabilities, allowing them to endure high average output levels [1]. The availability of high-brightness pump sources, combined with the utilization of large-mode-area (LMA) step-index fibers (SIFs), has propelled the output power of high-power fiber laser systems to multi-kilowatt levels [2,3]. However, this impressive evolution in power scaling also leads to increased thermal load. The thermal lensing (TL) effect, characterized by a reduction in mode field diameter (MFD) as the average output power rises, intensifies the impact of nonlinear effects while diminishing the advantages of large-mode-diameter designs [4].

More recently, a new thermally induced nonlinear effect known as transverse mode instability (TMI) has been identified. The threshold for this effect is dependent on the average power of high-power fiber lasers (HPFLs). Once a certain average power is reached, a sudden onset of temporal fluctuations in the beam profiles occurs, which degrades the output beam quality and halts further increases in output power. It is generally believed that this instability arises from the dynamic energy transfer between the fundamental mode (FM) and the higher-order modes (HOMs), with the onset of this effect being triggered by thermal grating [5]. Numerous advanced numerical models have been proposed, providing significant insight into the TMI effect and guiding efforts to improve the TMI threshold [6–9]. Among these models, the TMI coupling coefficient is a critical parameter that determines the mode coupling gain and quantifies the strength of the TMI effect. This coefficient is highly dependent on the mode profiles of the FM and HOMs, as well as the frequency shift

between them. As long as the mode functions and thermal Green's function for a fiber are determined, the TMI coefficient can be calculated, allowing for the determination of the TMI threshold for a specific fiber [6,7].

In fiber amplifier systems, fibers are often bent or coiled to a selected diameter, a practice that aims to suppress unwanted HOMs and enhance the output beam quality. Both theoretical and experimental studies have demonstrated that optimizing the fiber's bending radius and coiling method can improve the TMI threshold [10]. These investigations primarily consider the bending-induced mode losses in HOMs. However, it is essential to recognize that bending the fiber also alters the mode profiles that the fiber can support, which in turn impacts the TMI coupling coefficient—a factor that should not be overlooked. Furthermore, as power levels increase, the TL effect compresses the modes guided by the bent fiber, leading to further modifications of the TMI coefficient. The combined effect of bending and TL-induced changes in the mode profile on TMI has yet to be thoroughly investigated.

Herein, we present a numerical analysis of the impact of mode distortion caused by the combined effects of bending and TL on the TMI coefficient in conventional large-core step-index fibers with core/cladding diameters of 20/400 μm and 25/400 μm. Bending radii were selected in a range where the FM experiences negligible loss while the LP11 mode exhibits less than 1 dB/m of bend loss. A heat load of 200 W/m was applied to assess its effect. The numerical results suggest that the increased heat load appears to contribute to a reduction in mode loss for the bent fiber; the mode distortion resulting from both bending and TL within the specified bending radius and heat load ranges does not significantly influence the TMI coefficient.

2. Theoretical Background and Simulation Method

To begin, we provide a brief overview of the theoretical background underpinning our model. Following this, we outline the simulation process, detailing the calculation methods employed at each stage of the model.

The mode coupling mechanism is believed to be a form of stimulated thermal Rayleigh scattering (STRS); the theoretical model of STRS has been widely employed in TMI studies [6–8,11]. In the model [8], the simplified output power of HOM (LP11 in this article) with a fiber length of L derived from the coupling equations is

$$P_{11}(L) = P_{11}(0)e^{(g_{11}-\alpha_{11})L}e^{\chi P_{01}(L)}, \quad (1)$$

where α_{11} is the mode loss of LP_{11}. $P_{11}(0)$ and $P_{01}(L)$ are the initial power of the LP_{11} mode and the output power of the FM (LP_{01} mode), respectively. χ denotes the TMI coupling coefficient between the LP_{01} mode and LP_{11} mode. $g_{11} = g\Gamma_{11}$ represents the propagation distance-independent fiber amplifier gain for LP_{11} modes; g is the rare earth doping-raised bulk gain coefficient. Γ is the overlap integral between the doped region and the transverse modes, which can be written as $\Gamma_i = \iint_{S_d} \psi_i(r_\perp)^* \psi_i(r_\perp) d^2 r_\perp$, where $\psi_i(r_\perp)$ represents the mode profile, S_d and the subscript denote the doped region and transverse coordinates x and y, and the outer integral is over the entire fiber cross-section.

From Equation (1), it is clear that the power growth of the LP_{11} mode is influenced by three key factors: the initial power of the LP_{11} mode ($P_{11}(0)$); the laser gain ($g_{11} - \alpha_{11}$), which encompasses both the amplification process and the total mode loss; and the mode coupling gain ($\chi P_{01}(L)$), which depends on the TMI coefficient and the output power of the LP_{01} mode. This understanding leads to three corresponding methods for TMI suppression: improving the mode purity of the LP_{01} mode, which can reduce the proportion of the initial power of LP_{11}; increasing the mode loss to filter the LP_{11} mode out and effectively diminish its growth by making it less competitive in terms of amplification; and reducing the TMI coefficient, weakening the mode coupling process. One practical approach to enhance mode-dependent loss is to bend the fiber at a smaller radius. This method is particularly effective, as HOMs such as LP_{11} typically experience greater bend loss compared to the FM. By carefully selecting the bending radius, it is possible to significantly suppress power

growth in HOMs without the need for modifications to fiber designs or adjustments to the wavelength [12,13].

Theoretical work analyzing the influence of fiber bending on the TMI threshold primarily focuses on the mode-dependent losses induced by bending, representing the second factor impacting TMI; however, it is important to recognize that bending the fiber also alters the mode profiles. Additionally, as power increases, the heat load resulting from quantum defect and photodarkening generates the TL effect, which modifies the refractive index distribution of the bent fiber and further alters the mode profiles. This interplay results in mode distortion, which affects the TMI coefficient and, consequently, influences the mode coupling gain—this constitutes the third factor we previously mentioned. In the following discussion, we will primarily examine how mode distortion affects the TMI coefficient and its implications for the TMI threshold. Since both bending-induced mode loss and mode distortion impact the TMI effect, we employ the semi-analytic model proposed by Hansen to isolate the effects of mode distortion due to bending. In this model, mode loss is not incorporated into the mode coupling equations, allowing us to focus on the pure impact of bending-induced mode distortion on the TMI; the equations are expressed as [6,7]

$$\frac{\partial P_{01}}{\partial z} = -\chi_1(\Delta\omega)g(z)P_{11}P_{01} + \Gamma_1 g(z)P_{01}, \tag{2a}$$

$$\frac{\partial P_{11}}{\partial z} = \chi_2(\Delta\omega)g(z)P_{11}P_{01} + \Gamma_2 g(z)P_{11}, \tag{2b}$$

where $\Delta\omega = \omega_1 - \omega_2$ is the frequency shift between LP_{01} and LP_{11}. The TMI coefficient χ is given by [6]

$$\chi_{1,2}(\Delta\omega) = \frac{\eta k^2}{\kappa\beta_2}\mathrm{Im}[B_{21}(\Delta\omega)]\left(1 - \frac{\lambda_s}{\lambda_p}\right), \tag{3}$$

The descriptions of the parameters used are listed in Table 1. The quantity B_{21} is determined by the Green's function $G(r_\perp, r'_\perp, \Delta\omega)$ of the fiber and the normalized fiber mode profiles $\psi_1(r_\perp)$ and $\psi_2(r_\perp)$ of the LP_{01} and LP_{11} mode, which can be expressed by

$$B_{21}(\Delta\omega) = \iint \psi_2(r_\perp)\psi_1(r_\perp)\iint_{S_d} G(r_\perp, r'_\perp, \Delta\omega)\psi_1(r'_\perp)\psi_2(r'_\perp)dr'_\perp r_\perp, \tag{4a}$$

$$G(r_\perp, r'_\perp, \omega) = G(r_\perp - r'_\perp, \omega), \tag{4b}$$

$$G(r_\perp - r'_\perp, \Delta\omega) = \frac{1}{2\pi}K_0\left(\sqrt{q(\Delta\omega)|r_\perp - r'_\perp|}\right), \tag{4c}$$

where $q = i\rho C\Delta\omega/\kappa$, and K_0 is the zeroth-order modified Bessel function of the second kind. For each fiber design for which the Green's function can be determined, the TMI coefficient can be calculated numerically using the mode functions of the coupled two modes and the frequency offset between them.

The schematic of the simulation process is illustrated in Figure 1. To obtain the mode profiles of the bent fiber considering the TL effect, the initial step is to calculate the mode profile based solely on bending. This mode profile serves as the source for determining the thermally induced refractive index changes at a specific heat load. Utilizing the new refractive index distribution, we can then simulate the modified mode profile that incorporates thermal effects for a given bending radius. Subsequently, the updated mode profile is treated as the new source to reevaluate the thermal-induced refractive index changes with an increased heat load. By iterating this calculation process, we can derive the mode profiles of the fiber affected by the TL effect for each specific bending radius. The numerical simulations were performed using the full-vectorial finite element method (FEM).

Table 1. Physical constants of the simulated fiber.

Symbol	Quantity	Value
D_c	Core diameter	20 µm, 25 µm
D_{cl}	Cladding diameter	400 µm
R_b	Bending radius	2.5–10 cm, 2–10 cm
NA	Numerical aperture	0.065
n_c	Core refractive index	1.45
λ_p	Pump wavelength	976 nm
λ_s	Operating wavelength	1064 nm
h_q	Convection coefficient of the cooling fluid	1000 W/(m^{2}K)
η	Thermo-optic coefficient	3.5×10^{-5} K^{-1}
κ	Thermal conductivity	1.4 W/(K m)
ρC	Product of density and specific heat capacity	1.67×10^6 J/(Km^3)
c	Light speed	3×10^8 m/s
$\hbar$	Reduced Planck constant	$6.63 \times 10^{-34}/(2\pi)$

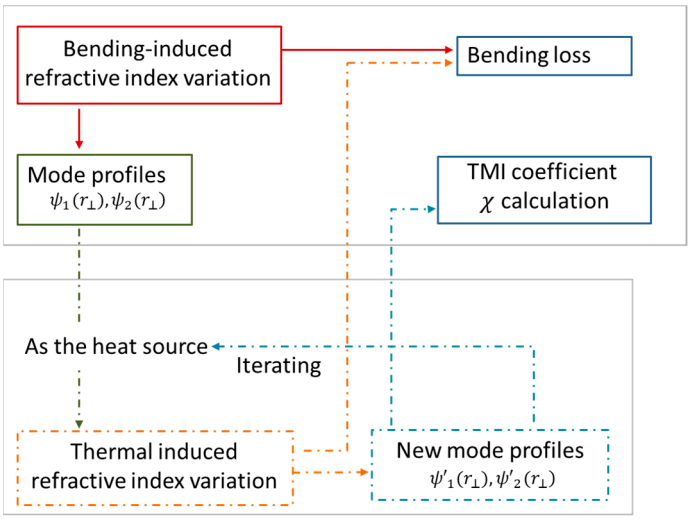

Figure 1. The outline of the simulation process.

We begin by investigating the bending characteristics of the LMA step-index fiber to determine its refractive index distribution under bending conditions. To achieve this, we transform the bent fiber into an equivalent straight fiber using conformal mapping and coordinate transformation, as suggested in [10]:

$$n_{eq}(x,y) = n(x,y)\exp(\frac{x}{R_{eff}}) \approx n(x,y)(1+\frac{x}{R_{eff}}), x \ll R, \quad (5)$$

where $n_{eq}(x,y)$ is the equivalent refractive index profile of the straight fiber under the bending condition; $n(x,y)$ is the refractive index distribution of the straight fiber; and R_{eff} is the effective bending radius. For silica fiber, $R_{eff} = 1.28R$. Thus, the modified refractive index for various bending radii can be obtained, allowing us to determine the corresponding mode profile distribution. The bending loss can then be calculated based on the imaginary part of the effective index n_{eff} [14].

$$2\alpha[dB/m] = \frac{20}{ln(10)}\frac{2\pi}{\lambda}\mathrm{Im}\{n_{eff}\}, \quad (6)$$

The effective areas calculated from the mode field distribution at the different bending radii are given by

$$A_{eff} = \frac{\left(\iint |\psi(\mathrm{r}_\perp)|^2 \mathrm{d}^2\mathrm{r}_\perp\right)^2}{\iint |\psi(\mathrm{r}_\perp)|^4 \mathrm{d}^2\mathrm{r}_\perp}, \tag{7}$$

Subsequently, the mode field distribution obtained from the bent fiber is utilized to study the thermally induced variations in the refractive index. The heat generated during the amplification process leads to a thermal distribution within the fiber, which is crucial for understanding the changes in the refractive index resulting from the thermal-optic effect: $\beta = dn/dT$, where β is the thermal-optic coefficient. To simplify the analysis, we assume that heat deposition within the fiber is uniform and occurs solely in the doped core region. The cladding region is considered to possess the same thermal properties as the core. For this analysis, we will neglect the coating region. By solving the heat diffusion equation under steady-state conditions, we can derive the expressions for the thermal distribution $T(r)$ in both the core and cladding regions. Combined with the proportional relationship between the refractive index variation and temperature variation given by $\Delta n_\beta(r) = \beta(T(r) - T_c)$, where T_c is the coolant temperature, the refractive index distribution under different heat load can be expressed as [1,14]

$$n_T(q,r) = \begin{cases} n_{co} + \beta\left[\frac{q_h(a^2-r^2)}{4k_{si}} + \frac{q_h a^2}{2k_{si}} \ln\left(\frac{b}{a}\right)\right], 0 \le r \le a \\ n_{cl} + \beta\left[\frac{q_h a^2}{2k_{si}} \ln\left(\frac{b}{r}\right)\right], a \le r \le b \end{cases}, \tag{8}$$

where the heat power density $q_h = Q/\pi a^2$, and Q denotes the heat load along with the fiber. a and b are the core and cladding radii; n_{co} and n_{cl} are the refractive index of core and cladding; k_{si} stands for the thermal conductivity of silica; and h_q is the convective coefficient. The refractive index distribution of the fiber under increased heat load at a specific bending radius can then be calculated after conformal mapping and coordinate transformation as in Equation (5):

$$n_T(q,x) = \begin{cases} \left(n_{co} + \beta\left[\frac{q_h(a^2-x^2)}{4k_{si}} + \frac{q_h a^2}{2k_{si}} \ln\left(\frac{b}{a}\right)\right]\right)(1 + \frac{x}{R_{eff}}), 0 \le x \le a \\ \left(n_{cl} + \beta\left[\frac{q_h a^2}{2k_{si}} \ln\left(\frac{b}{x}\right)\right]\right)(1 + \frac{x}{R_{eff}}), a \le x \le b \end{cases}, \tag{9}$$

This allows for the determination of the corresponding mode profiles. By varying the bending radius, the mode profiles of the fiber affected by the thermal loading (TL) effect can be similarly obtained for each defined radius.

Using the mode field distributions of the bent fiber under the TL effect, the TMI (threshold for modal instability) coefficient can be calculated based on the previously provided expression, enabling the determination of the TMI threshold. In this analysis, we consider both quantum noise and intensity noise as the initial sources for the TMI process. For the quantum noise seeding (QNS), the HOM content is defined as [6]

$$\xi(L) \approx \hbar\omega_0 \sqrt{\frac{2\pi\Gamma_1}{|\chi''(\Omega_p)|}} \frac{P_1(L)^{\left(\frac{\Gamma_2}{\Gamma_1} - \frac{3}{2}\right)}}{P_{0,1}{}^{\frac{\Gamma_2}{\Gamma_1}}} \exp\left[\frac{\chi(\Omega_p)}{\Gamma_1}(P_1(L) - P_{0,1})\right], \tag{10}$$

where $P_{0,1}$ and $P_1(L)$ are the input power and the output power at the fiber length of L, and $\hbar\omega_0$ is a defined equivalent input power spectral density (PSD) of the quantum noise. Γ_1 and Γ_2 are the overlap integrals of FM and HOM. Ω_p is the frequency of the maximum χ, and χ'' is the second deviation value of χ with respect to Ω. With the given threshold HOM content of $\xi_{th} = 0.05$, the quantum noise-seeded TMI threshold power $P_1(L) = P_{th}$ can be solved correspondingly. For the case that the TMI is seeded by intensity noise, that is, in the situation that a small amount of signal exists in the LP_{11} mode due to the unperfect mode matching of signal light in the fiber, the fraction of HOM is given by [6]

$$\xi(L) \approx \xi(0)\left(\frac{P_{0,1}}{P_1(L)}\right)^{1-\frac{\Gamma_2}{\Gamma_1}}\left[1+\frac{1}{4}R_N(\Omega_p)\sqrt{\frac{2\pi\Gamma_1}{P_1(L)|\chi''(\Omega_p)|}}\exp\left(\frac{\chi(\Omega_p)}{\Gamma_1}P_1(L)\right)\right], \quad (11)$$

where the $\xi(0)$ is the assumed initial HOM content and $R_N(\Omega_p)$ is the relative intensity noise (RIN) of the input signal.

3. Results

Based on the model outlined in Section 2, a numerical simulation has been conducted on conventional LMA step-index fibers with diameters of 20/400 µm and 25/400 µm, which are commonly utilized in HPFL systems. The simulation focuses exclusively on the LP_{01} and LP_{11} modes, as the LP_{01} mode typically carries the highest power, while the interaction between the LP_{01} and LP_{11} modes exhibits the strongest coupling related to the TMI effect. The physical constants used in the calculations are detailed in Table 1.

The simulated refractive index profiles for both the straight fiber and the bent fiber (with a bending radius of 10 cm) under various heat loads are presented in Figure 2. It is observed that prior to applying the heat loads, the refractive index distribution of the bent fiber is tilted, increasing in the direction away from the bend. This bending-induced change in the index results in a shift in the mode outward from the core region and a concomitant reduction in the mode area. Upon the application of heat loads, the refractive index of both fibers rises with increasing thermal input; notably, the increment in the core region is greater than that in the cladding region. This differential increase enhances mode confinement, and the thermally induced variation in refractive index further reduces the size of the mode guided within the fiber. Figure 3 presents the corresponding simulated mode cross-sections of the LP01 mode and both orientations of the LP11 mode in straight fiber, bent fiber (with a bending radius of 10 cm), and thermally loaded bent fiber (with a heat load of 150 W/m @ 10 cm bending radius). As expected from the refractive index distribution, the mode field distributions of both LP01 and LP11 modes in the bent fiber are distorted and shift away from the core center. The two orientations of the LP11 mode lose the rotational symmetry observed in the straight fiber. When the thermal load is applied to the bent fiber, the mode profiles further shrink.

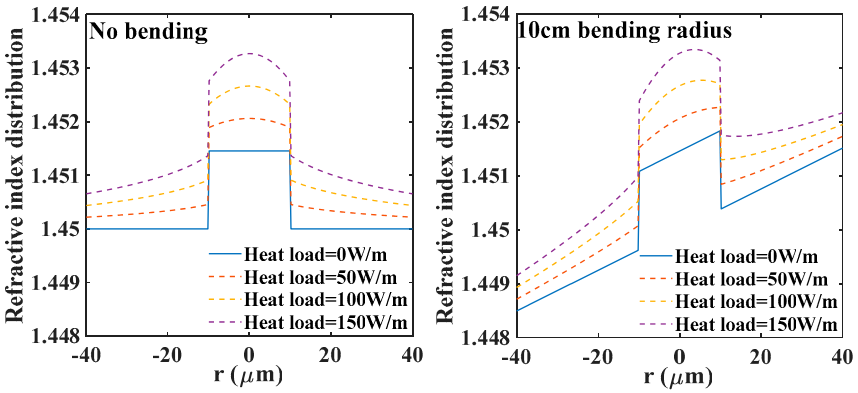

Figure 2. Refractive index profiles of the straight fiber and the bent fiber with a 10cm bending radius under various heat loads; the fiber core size is 20 µm.

In the following analysis of the TMI effect influenced by the combined impacts of thermal loading (TL) and bending-induced mode distortion, we first evaluate the evolution of mode loss in the fiber under various bending radii. This evaluation aims to identify an appropriate bending radius for further analysis of the thermal combined effect. Typically, the bending radius is selected to ensure that the fiber operates effectively in single-mode conditions, where the mode loss for LP_{01} remains minimal, thereby preserving the output power. This requires that the mode loss criteria be met, specifically that the loss of LP_{01} is less than 0.1 dB/m, while the loss of HOMs should exceed 10 dB/m. However, achieving this criterion is often challenging in practical systems. In our simulation, we established

more feasible limits for mode loss, setting the upper and lower bounds for LP_{01} and LP_{11} modes at 0.1 dB/m and 1 dB/m, respectively, resulting in a differential loss ratio of 10. This approach simplifies the satisfaction of the mode loss conditions. Furthermore, we focus exclusively on the least lossy orientation of the LP_{11} mode, as this configuration yields the lowest TMI threshold.

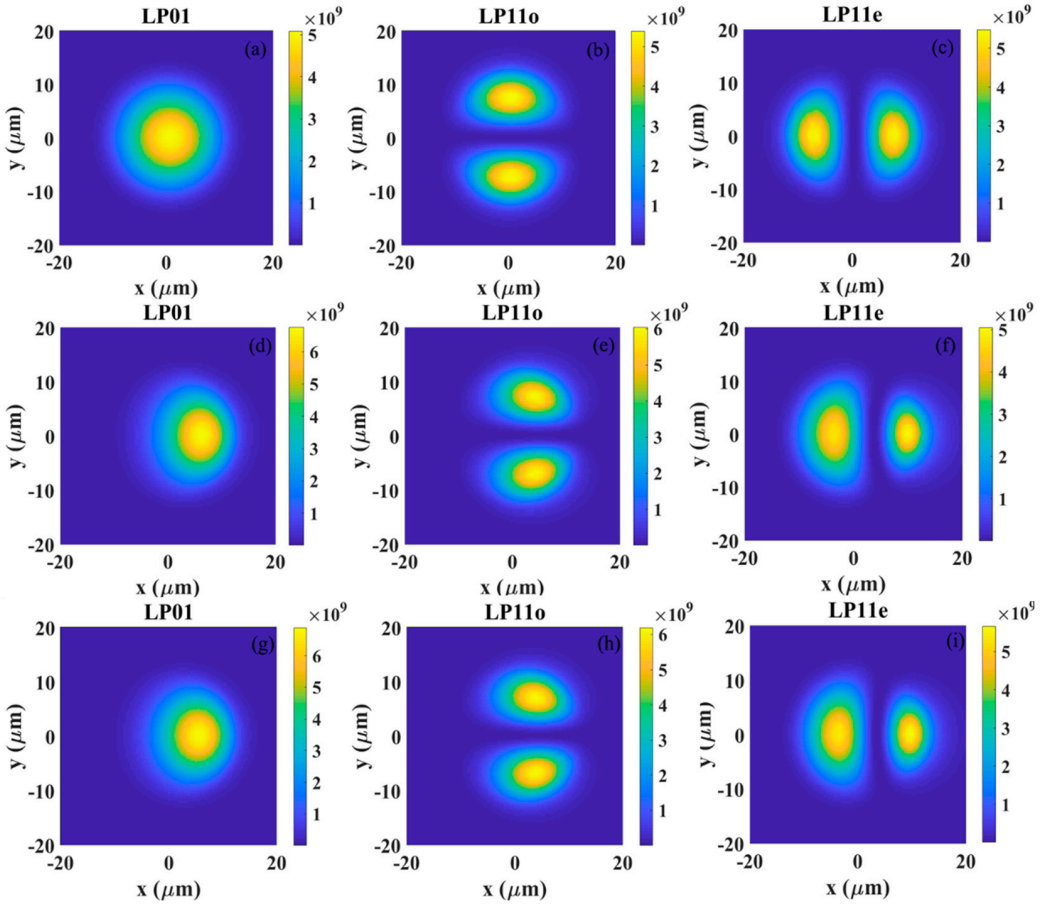

Figure 3. Simulated mode field distribution of LP_{01} and LP_{11} modes (**a**–**c**) in the straight fiber, (**d**–**f**) in the bent fiber, and (**g**–**i**) in the thermally loaded bent fiber.

In Figure 4, we present the mode loss variation for the LP_{01} (red dashed line in the corresponding red coordinate axes) and LP_{11} modes (solid red line) as a function of bending radius. Consistent with previous research [10], the LP_{11} mode experiences significantly higher bending loss compared to the LP_{01} mode. This characteristic allows for the effective stripping of the LP_{11} mode, thereby retaining the dominant LP_{01} mode by selecting an appropriate bending radius. For a fiber with a 20 μm core diameter, the bending loss of the LP11 mode is below 1 dB/m when the bending radius exceeds 4.8 cm, while the bending loss of the LP_{01} mode surpasses 0.1 dB/m when the bending radius falls below 3 cm. In the case of a fiber with a 25 μm core diameter, the LP_{11} bending loss remains under 1 dB/m for bending radii greater than 3.3 cm, whereas the LP_{01} loss exceeds 0.1 dB/m when the radius is less than 2.8 cm. Consequently, the optimal bending radii for the 20/400 μm fiber and the 25/400 μm fiber are 4.5 cm and 3.25 cm, respectively, where the corresponding bending losses at these specific radii are 3×10^{-4} dB/m (LP_{01}) and 1.8 dB/m (LP_{11}) for the first fiber and 3.3×10^{-2} dB/m (LP_{01}) and 1.8 dB/m (LP_{11}) for the second fiber. The mode loss evolution of the LP_{11} mode as a function of heat load at this specific bending radius for both fibers is also illustrated with the blue line on the corresponding blue coordinate axes. It is observed that the mode losses of the LP_{11} mode in both fibers decrease with the increasing heat load. For the 20/400 μm fiber, the LP_{11} mode loss drops below 1 dB/m when the heat load exceeds 21 W/m (approximately 253 W of absorbed pump power).

Similarly, for the 25/400 μm fiber, the LP_{11} mode loss falls below 1 dB/m when the heat load exceeds 31 W/m (approximately 373 W of absorbed pump power). This finding indicates that the mode loss criteria necessary for stripping higher-order modes (HOMs) in the fiber may no longer be satisfied when the heat load on the bent fiber increases beyond a certain threshold.

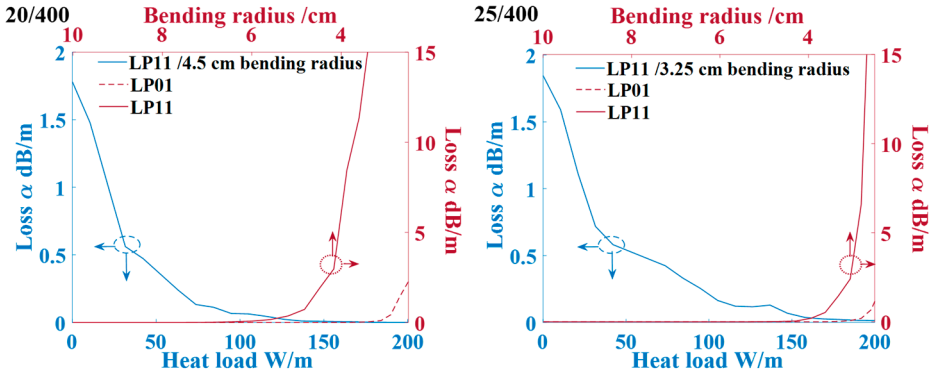

Figure 4. Mode loss evolution of LP_{01} and LP_{11} modes as a function of bending radius (red line with red axes, as the red arrows indicated) and mode loss evolution of LP_{11} mode as the function of heat load under specific bending radius (blue line with blue axes, as the blue arrows indicated) of fiber with a 20 μm core size and a 25 μm core size, respectively.

Figure 5 illustrates the evolution of the effective area of the LP01 mode as a function of bending radius (red line on the red axes) and the effective area in response to heat load at each fiber's specific bending radius (blue line on the blue axes). As the bending radius decreases, the effective area diminishes due to changes in the refractive index. Moreover, under specific bending radii, the effective area of the LP01 mode contracts linearly with increased heat load. For the 20/400 μm fiber, at a bending radius of 4.5 cm and a heat load of 21 W/m, the effective area decreases by approximately 4.3% compared to that in the undisturbed state. In the case of the 25/400 μm fiber, at a bending radius of 3.25 cm and a heat load of 31 W/m, the effective area shrinks by about 16.7% relative to its original value. Notably, the effective area reduction is more pronounced in the larger-core-size fiber when both fibers are subjected to the same bending and heat-loading conditions.

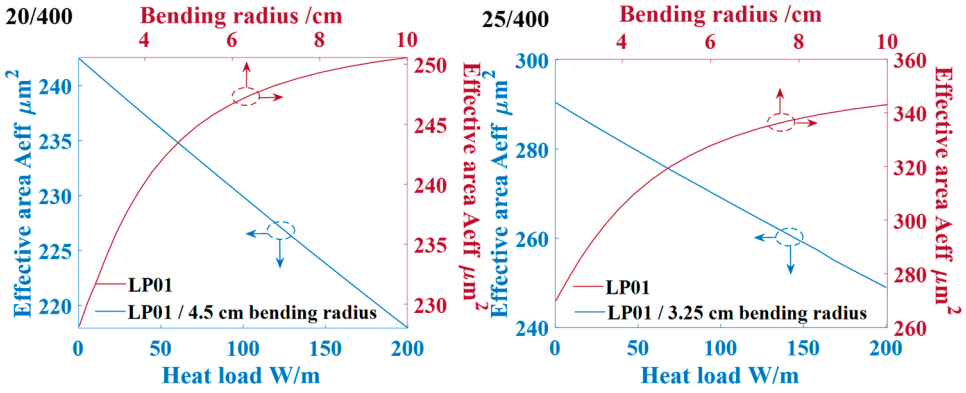

Figure 5. Effective area evolution as a function of bending radius (red line with red axes, as the red arrows indicated) and effective area evolution as the function of heat load under specific bending radius (blue line with blue axes, as the blue arrows indicated) of the LP_{01} mode in fibers with a 20 μm core size and a 25 μm core size, respectively.

By analyzing the simulated mode field distributions under various bending radii and heat loads at a specific bending radius, we can derive the TMI coefficient. As illustrated in Figure 4, the bending losses for the LP_{11} mode are minimal when the bending radius exceeds 8 cm for both types of fiber, making it reasonable to assume that the fibers are in a

relaxed state. In Figure 6, we compare the TMI coefficients for LP_{01}-LP_{11} coupling of the fiber in this relaxed state against their respective TMI coefficients at specific bending radii without any heat load, as well as those under a heat load of 200 W/m (specifically, 4.5 cm for the 20/400 μm fiber and 3.25 cm for the 25/400 μm fiber). It is observed that, in the absence of heat load, the TMI coefficient decreases as the bending radius approaches the specified radius for each fiber. When each fiber is bent to its specific bending radius, the TMI coefficient experiences a slight increase as the heat load rises to 200 W/m. To further investigate the trend of TMI coefficient variations, we plot the peak TMI coefficient as a function of bending radius (represented by the red line on the red coordinate axes) and the peak TMI coefficient as a function of heat load in the bent fibers (illustrated by the blue line on the blue coordinate axes) in Figure 7. It is evident that there is a significant decrease in the peak TMI coefficient with a tighter bending radius when the radius is less than 4 cm. For the 20/400 fiber, the peak TMI coefficient decreases by approximately 3.7% when the bending radius tightens from 10 cm to 4.5 cm, while the 25/400 fiber shows a reduction of about 4.2% in the peak TMI coefficient when the bending radius is reduced from 10 cm to 3 cm. As the heat load increases to 200 W/m, the peak TMI coefficient exhibits differing trends in the two fiber types: there is a 1.24% increase in the 20/400 fiber and a 1.48% decrease in the 25/400 fiber. Overall, the influence of the tightening bending radius on the TMI coefficient is more pronounced than the effect of the thermal load on the bent fibers.

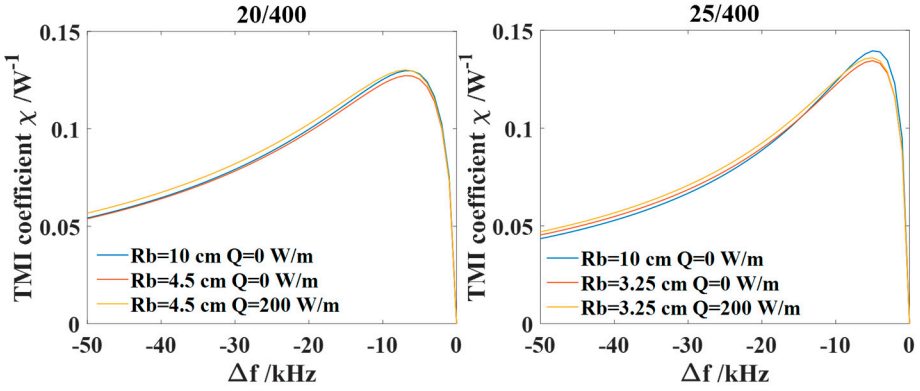

Figure 6. TMI coefficient χ for LP01-LP11 coupling as a function of the frequency shift for varying bending radii with no heat load and varying heat load without bending of two fibers.

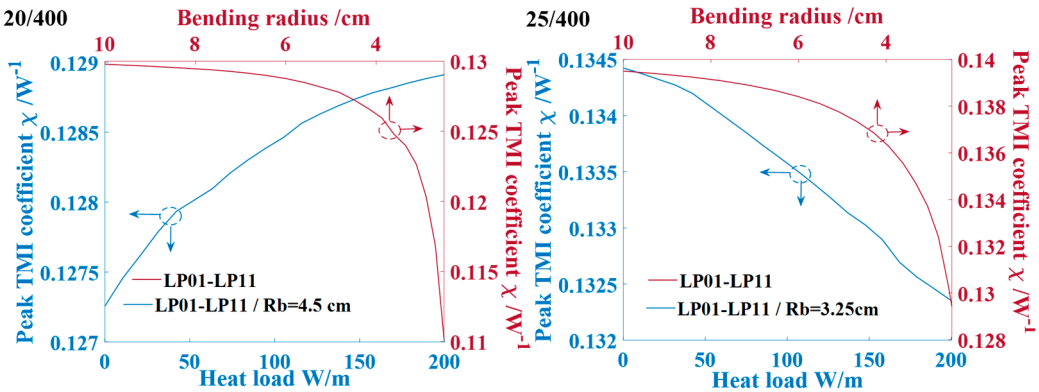

Figure 7. The peak TMI coefficient χ for LP01-LP11 coupling as a function of bending radius for the two fibers (red line with red axes, as the red arrows indicated) and peak TMI coefficient χ for LP01-LP11 coupling as a function of heat load under the specific bending radius for each fiber (blue line with blue axes, as the blue arrows indicated).

Finally, we calculated the TMI threshold for two fibers under the same conditions established in the TMI coefficient analysis. This analysis focuses exclusively on the pure impact of mode distortion on the TMI threshold, without accounting for mode loss. The

threshold for the higher-order mode (HOM) content was set to 0.05. We analyzed both cases in which TMI was seeded by quantum noise (QNS) and intensity noise (INS). For all cases, the input power was maintained at 1 W, with an initial HOM content and a relative intensity noise (RIN) of 10^{-10} Hz^{-1} for the case of signal intensity noise seeding. The output HOM content as a function of output power for both QNS and INS is depicted in Figure 8. The results indicate that tighter bending of the fibers leads to a higher TMI threshold for both QNS and INS. For the 20/400 μm fiber, when the bending radius was reduced from 10 cm to 4.5 cm, the TMI threshold increased from 223 W to 226 W for QNS and from 116 W to 118 W for INS. For the 25/400 μm fiber, when the bending radius decreased from 10 cm to 3.25 cm, the TMI threshold increased from 213 W to 216 W for QNS and from 112 W to 114 W for INS. Under bending conditions, with a 4.5 cm bending radius for the 20/400 μm fiber and a 3.25 cm bending radius for the 25/400 μm fiber, an increase in heat load to 200 W/m resulted in a decline in the TMI threshold for the 20/400 μm fiber, which dropped from 226 W to 223 W for QNS and from 118 W to 117 W for INS. In contrast, for the 25/400 μm fiber, the TMI threshold changed slightly, from 216 W to 217 W, for QNS while remaining unchanged for INS. These observations indicate that bending-induced mode distortion can lead to a slight improvement in the TMI threshold; when combined with the TL effect, this slight improvement will then be weakened. In comparison with the impact of mode loss on the TMI threshold, the effects caused by mode distortion from bending and TL in bent fibers are minor.

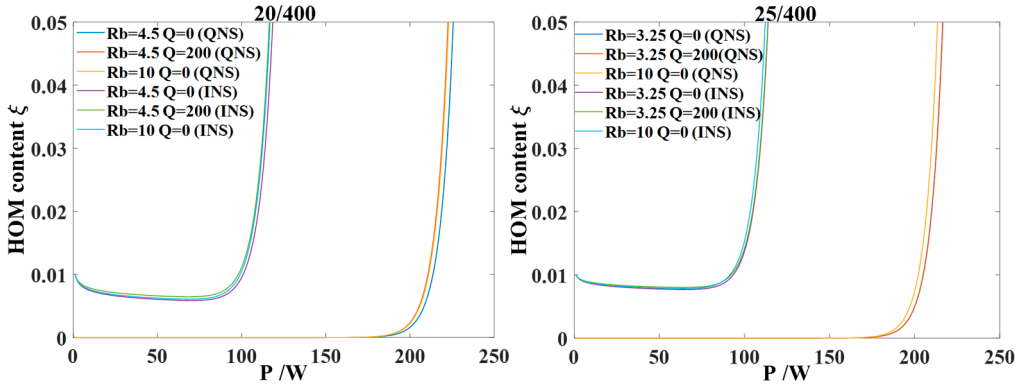

Figure 8. The output HOM content as a function of output power for intensity noise seeding (INS) and quantum noise seeding (QNS) under varying bending radii and varying heat loads for 20/400 μm fiber and 25/400 μm fiber.

4. Conclusions

In summary, we conducted a numerical analysis of the influence of the TMI effect, focusing on the mode distortion caused by bending and the combined effects of bending and TL in 20/400 and 25/400 LMA step-index fibers. The bending radii for the two fibers were selected to ensure that the fibers operated effectively in single-mode conditions. The simulation results indicated that increased thermal load on the bent fiber can actually reduce bending loss. Moreover, mode distortion induced by bending can alter the TMI coefficient, whereby tighter bends are associated with a lower peak TMI coefficient and a slightly elevated TMI threshold. Notably, the mode distortion caused by TL in the bent fiber did not have a significant impact on the TMI coefficient, and the TMI threshold remained relatively insensitive to the TL effects in the bent fibers at the selected bending radii and the given maximum thermal load applied to both fiber types.

Author Contributions: Conceptualization, D.C., Q.Z. and Y.F.; methodology, D.C., Q.Z. and Y.F.; software, D.C., Q.Z. and Y.F.; validation, D.C., Q.Z. and Y.F.; formal analysis, D.C., Q.Z. and Y.F.; investigation, K.Z. and Z.C.; resources, K.Z.; data curation, Y.F., K.Z. and Z.C.; writing—original draft preparation, D.C., Q.Z. and Y.F.; writing—review and editing, D.C., Q.Z. and Y.F.; visualization, Y.F.; supervision, Y.F. and K.Z.; project administration, K.Z. and Z.C; funding acquisition, K.Z., Z.C., D.Z. and H.Z. All authors have read and agreed to the published version of the manuscript.

Funding: This research was funded by the foundation of the Key Laboratory of Science and Technology for National Deference.

Institutional Review Board Statement: Not applicable.

Informed Consent Statement: Not applicable.

Data Availability Statement: Data are unavailable due to privacy restrictions.

Conflicts of Interest: The authors declare no conflicts of interest.

References

1. Brown, D.C.; Hoffman, H.J. Thermal, stress, and thermo-optic effects in high average power double-clad silica fiber lasers. *IEEE J. Quantum Electron.* **2001**, *37*, 207–217. [CrossRef]
2. Nilsson, J.; Payne, D.N. High-Power Fiber Lasers. *Science* **2011**, *332*, 921–922. [CrossRef] [PubMed]
3. Richardson, D.J.; Nilsson, J.; Clarkson, W.A. High power fiber lasers: Current status and future perspectives. *J. Opt. Soc. Am. B* **2010**, *27*, B63–B92. [CrossRef]
4. Dong, L. Thermal lensing in optical fibers. *Opt. Express* **2016**, *24*, 19841–19852. [CrossRef] [PubMed]
5. Jauregui, C.; Stihler, C.; Limpert, J. Transverse mode instability. *Adv. Opt. Photonics* **2020**, *12*, 429–484. [CrossRef]
6. Hansen, K.R.; Alkeskjold, T.T.; Broeng, J.; Lægsgaard, J. Theoretical analysis of mode instability in high-power fiber amplifiers. *Opt. Express* **2013**, *21*, 1944–1971. [CrossRef] [PubMed]
7. Hansen, K.R.; Alkeskjold, T.T.; Broeng, J.; Lægsgaard, J. Thermally induced mode coupling in rare-earth doped fiber amplifiers. *Opt. Lett.* **2012**, *37*, 2382–2384. [CrossRef] [PubMed]
8. Dong, L. Stimulated thermal Rayleigh scattering in optical fibers. *Opt. Express* **2013**, *21*, 2642–2656. [CrossRef] [PubMed]
9. Tao, R.; Wang, X.; Zhou, P. Comprehensive Theoretical Study of Mode Instability in High-Power Fiber Lasers by Employing a Universal Model and Its Implications. *IEEE J. Sel. Top. Quantum Electron.* **2018**, *24*, 1–19. [CrossRef]
10. Schermer, R.T.; Cole, J.H. Improved Bend Loss Formula Verified for Optical Fiber by Simulation and Experiment. *IEEE J. Quantum Electron.* **2007**, *43*, 899–909. [CrossRef]
11. Tao, R.; Ma, P.; Wang, X.; Zhou, P.; Liu, Z. Study of dopant concentrations on thermally induced mode instability in high-power fiber amplifiers. *Laser Phys.* **2016**, *26*, 065103. [CrossRef]
12. Tao, R.; Su, R.; Ma, P.; Wang, X.; Zhou, P. Suppressing mode instabilities by optimizing the fiber coiling methods. *Laser Phys. Lett.* **2016**, *14*, 025101. [CrossRef]
13. Zhang, F.; Xu, H.; Xing, Y.; Hou, S.; Chen, Y.; Li, J.; Dai, N.; Li, H.; Wang, Y.; Liao, L. Bending diameter dependence of mode instabilities in multimode fiber amplifier. *Laser Phys. Lett.* **2019**, *16*, 035104. [CrossRef]
14. Kong, L.; Leng, J.; Zhou, P.; Jiang, Z. Thermally induced mode loss evolution in the coiled ytterbium doped large mode area fiber. *Opt. Express* **2017**, *25*, 23437–23450. [CrossRef] [PubMed]